ISSN 0869-5911, Petrology, 2006, Vol. 14, No. 6, pp. 588–608. © Pleiades Publishing, Inc., 2006.
Original Russian Text © A.I. Kiselev, V.V. Yarmolyuk, K.N. Egorov, R.A. Chernyshov, A.V. Nikiforov, 2006, published in Petrologiya, 2006, Vol. 14, No. 6, pp. 626–648.

Middle Paleozoic Basic Magmatism of the Northwestern Vilyui Rift: Composition, Sources, and Geodynamics

A. I. Kiselev[a], V. V. Yarmolyuk[b], K. N. Egorov[a], R. A. Chernyshov[b], and A. V. Nikiforov[b]

[a] *Institute of the Earth's Crust, Siberian Division, Russian Academy of Sciences, ul. Lermontova 128, Irkutsk, 664033 Russia*
e-mail: akiselev@crust.irk.ru

[b] *Institute of Geology of Ore Deposits, Petrography, Mineralogy, and Geochemistry (IGEM), Russian Academy of Sciences, Staromonetnyi per. 35, Moscow, 119017 Russia*
e-mail: volya@igem.ru

Received May 11, 2005

Abstract—Middle Paleozoic magmatism at the eastern Siberian platform was related to riftogenic processes, which were most clearly expressed in the Vilyui Rift and led to the formation of rift depressions filled with sedimentary–volcanogenic rocks and extended basaltic dike belts in rift shoulders. Two fields of diamondiferous kimberlites were found along with basaltic dikes in the Vilyui–Markha dike belt surrounding rift in the northwest. Active subalkali basaltic magmatism predated the emplacement of kimberlite bodies, which occasionally (Nyurba pipe) are cut by dikes of potassium alkali basalts. Based on geochemical and Sr–Nd isotopic characteristics, deep-seated sources were determined for the intrusive and volcanic basalts of the northwestern shoulder of the Vilyui rift. The REE distribution patterns of the studied rocks normalized to the primitive mantle are close to that of OIB, except for somewhat higher HREE. In the diagrams of indicator ratios of trace and rare-earth elements, the basalts are also plotted in the OIB field, being located between the end member of plume composition (FOZO) and enriched mantle sources. The rocks have positive ε_{Sr} (+3.5 and +28.6) and ε_{Nd} (+1. 3 and +5.3). In a diagram $\varepsilon_{Nd}(T)$–$\varepsilon_{Sr}(T)$, two fields with distinct content of radiogenic Sr are distinguished, which can be regarded as derived by mixing of the moderately depleted PREMA-type mantle and a source enriched in radiogenic Sr. Available isotope–geochemical data confirm that OIB type basalts of the region were generated by plume activity. The geodynamic setting of Middle Paleozoic magmatism and rifting in the eastern part of the Siberian platform is considered in light of plume–lithosphere interaction. The sequence of tectonomagmatic events during evolution of the Vilyui rift is consistent with the model of plume–lithosphere interaction or the model of active rifting.

DOI: 10.1134/S0869591106060051

INTRODUCTION

During Phanerozoic, the territory of the Siberian platform was repeatedly involved in within-plate activity, which generated flood basalts, systems of rifts and aulacogens, dike swarms, kimberlite fields and belts of alkaline massifs. One of the most significant manifestations of this activity was the formation of the Vilyui Rift (or aulacogen). It is believed (Zonenshain et al., 1990) that the rift evolved as an inland branch of a rift triple junction, while two other branches broke up the eastern (in the present-day coordinates) margin of the Siberian platform. Its formation was associated with intense magmatism varying in composition from basalt to kimberlite and carbonatite. This magmatism is of great importance in view of the giant volume of igneous rocks and their relations with important mineral resources of, for example, diamonds. However, some fundamental problems in the magmatic evolution of the Vilyui Rift remain unsolved. These are the nature of magmatic sources, causes of the change and evolution of magmatic melts with time, and the geodynamic processes responsible for the formation of aulacogen and magmatic activity. In this paper, we attempted to settle these problems based on Sr–Nd isotopic and geochemical data on the magmatic rocks developed in the northwestern shoulder of the Vilyui aulacogen (rift). This part of the rift area is distinct in showing a combination of kimberlite and basic magmatism, which is of interest in light of the problem of the deep-seated sources and geodynamic settings of such magmatism in the southeastern Siberian craton.

GEOLOGICAL SETTING

The Vlyui rift is located in the northeastern part of the Siberian platform and involves a system of depressions filled with volcanogenic–sedimentary sequences with a total thickness of up to 6 km. The geological age of the sequences is estimated at the Middle–Late Devonian. They are made up of the basaltic flows intercalating with terrigenous and carbonate rocks. All of these stratified rocks dip gently but were strongly deformed

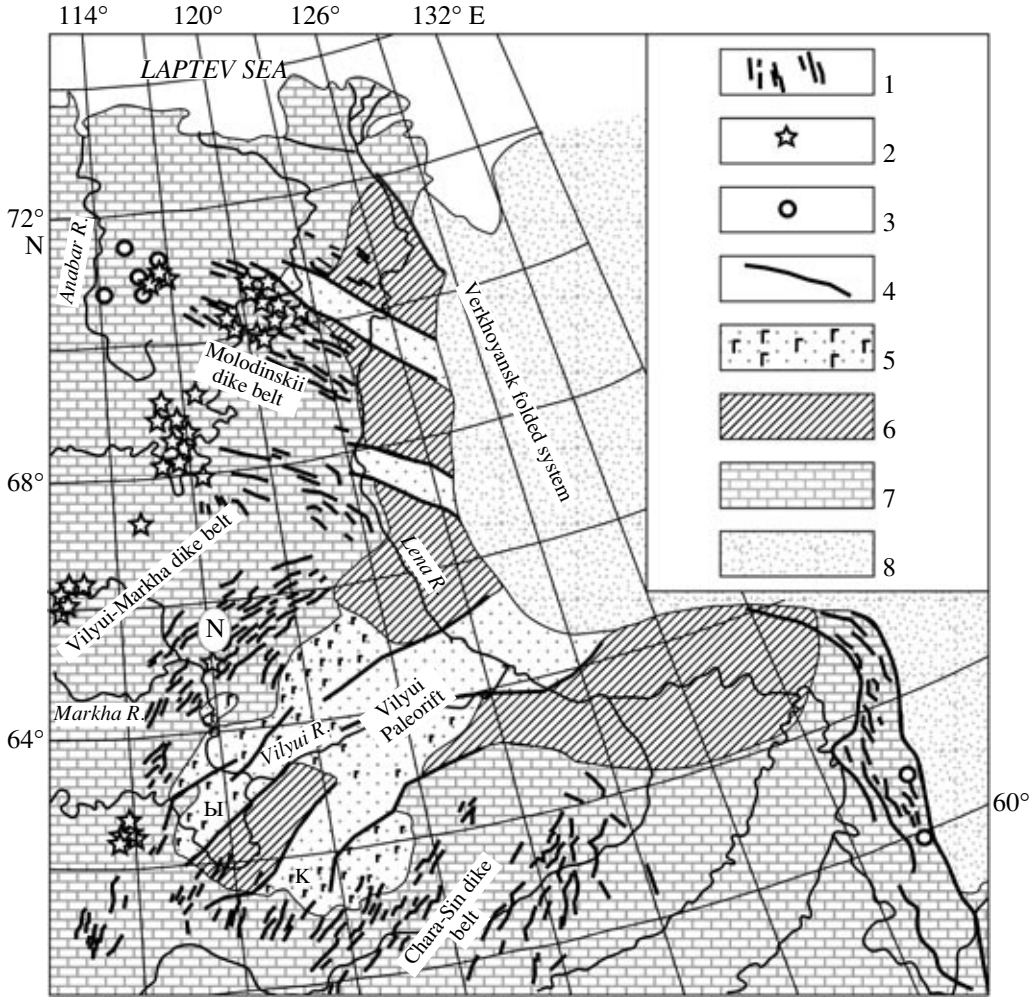

Fig. 1. Geological scheme of the Middle Paleozoic Vilyui Rift system.
(1) Basic dikes, (2) kimberlites, (3) massifs of the alkali ultramafic rocks and carbonatites, (4) faults, (5) volcanic–sedimentary sequences of rift depressions, (6) areas of relative rise (relicts of paleoarch), (7) Siberian platform, (8) Verkhoyansk folded system. (N) Nakyn kimberlite field, (Y, K) are Ygyatta and Kempendyai depressions.

by normal and reverse faults. Fault deformations were mainly caused by rift inversion in Early Carboniferous. Paleovolcanological reconstructions show that lava flows were accumulated in lagoonal shallow-water environments or at a peneplained island surface. The flows are from few meters to 10–20 m thick and up to a few tens kilometers long, composing units up to a few hundreds meters thick. In the Ygyatta depression (Fig. 1), the flows are made up of various basalts, occasionally plagiophyric or megaplagiophyric varieties (Appain Formation, D_3).

A distinctive feature of the Vilyui rift is two large dike swarms. They are most abundant in rift surrounding, in particular, in its eastern and northwestern shoulders, where they compose, respectively, the Chara–Sin and Vilyui Markha dike belts (Fig. 1). The latter belt and related magmatic rocks are the subjects of this paper. It is controlled by the large Vilyui–Markha fault system 700 km long and up to 30 km wide in the southwest and 70 km wide in the northeast. The belt consists of dikes and dike-shaped bodies of moderately alkaline basalts among the Upper Cambrian and Lower Ordovician sequences. Sills and chonoliths are less common. Dikes from 2 to 30 km long have an en-echelon structure, and northeastern or, more rarely, northwestern and submeridional strikes. The thickness varies from a few to 50–80 and more meters. Beneath the Jurassic deposits, the dikes are deciphered as linear magnetic anomalies of variable contrast.

The dikes are mainly monophase dolerite bodies. Complex bodies varying in composition from olivine dolerites to monzonite porphyries are less common. Among numerous mafic dikes of the Nakyn Field, only two dikes consist of dolerites and monzonite porphyries. One of the bodies found near the Nyurba pipe consists of two phases, with dolerites in marginal zones and monzonite porphyries in the core.

The sills of the dike complex are located at different levels of the platform cover, and their thicknesses vary from a few to ten few meters. The Mirninskoe kimberlite field contains equant bodies of explosion breccias ("basic diatremes"), along with sills and dikes. Some of them are spatially related to kimberlite bodies, while others are spaced at significant (10–30 km and more) distance. In many events, the diatremes are confined to the NE-trending faults controlling dolerite dikes. In the Nakyn field, the "explosion breccia" is associated with post-kimberlite dikes of alkali potassium basic rocks (Kiselev et al., 2002, 2004).

Kimberlites within the Vilyui–Markha dike belt form two pipe groups known as the Mirninskoe (Malaya Botuoba) and Nakyn fields spaced 300 km. It should be noted that kimberlites are located on the rift shoulders beyond the subsidence zone, i.e., where riftogenic processes were weakly expressed.

Of special interest is the problem of spatial association of kimberlite and basaltic magmatism. Their relations were described for the Mir pipe, in which kimberlites cut across two sills located at different depths and dike of Middle Paleozoic dolerites (Khar'kiv et al., 1997). The relations between these rocks can be illustrated by the example of the Nyurba kimberlite pipe (Nakyn field), which merges with aforementioned complex dolerite–monzonite porphyry body at a depth of 378 m (borehole 9/198) and is cut by alkali potassium basalts (Fig. 2). Based on finding of dolerite xenoliths in autolithic kimberlite breccia at a depth of 240–270 m, the temporal sequence of Middle Paleozoic magmatism in the region is as follows: dolerites of the dike belt—kimberlites–locally occurring alkali potassium basites.

Geological–stratigraphic data and isotope dating indicate that plutonic and volcanic basic rocks were formed during several magmatic pulses over the time span from the Middle Devonian through Early Carboniferous. The general sequence in the formation of volcanic rocks is deciphered from their stratigraphic position in the Middle Paleozoic succession. Outpouring of the basalts occurred in two stages: (1) Appain stage in the late Middle–early Late Devonian and (2) Emyaksin stage in the Late Devonian (Masaitic et al., 1975). The volcanic facies of basic rocks is located within Middle Paleozoic rift depressions southeast of the Vilyui–Markha dike belt (Fig. 1).

Dolerite dikes were presumably formed repeatedly throughout the entire period of volcanic activity. The earliest of them are supposedly dolerite dikes in the axial part of the Vilyui Rift, which were related to the initial phases of its opening. Dikes in the rift shoulders were formed either simultaneously with outpouring or after it. The attenuation of subaerial volcanism in the region occurred in the Late Devonian, when thick carbonate–terrigenous sequence and evaporites of the Upper Devonian–Lower Carboniferous continued to accumulate (Gaiduk, 1988). Kimberlite volcanism in the region also occurred in the Upper Devonian–Lower Carboniferous. Two age determinations of dolerites from the dike in the Botuoba fault taken within the depth interval of 95–104 m strongly differ: 353 ± 5 Ma (95–101 m) and 338 ± 5 Ma (101–104 m). The ages were determined by the K–Ar whole-rock method by D. P. Gladkochub. The youngest rocks (boundary of the Early and Middle Carboniferous) are dikes of alkali potassium basalts and monzonite porphyries, which can be related to the inversion movements along sublatitudinal faults in the rift. Based on the K–Ar determinations made by S. B. Brandt and I. S. Brandt at the Institute of the Earth's Crust, Russian Academy of Sciences, the age of post-kimberlite basalts of the Nyurba pipe was 320 Ma.

The K–Ar, Ar–Ar, Rb–Sr, and Sm–Nd dates for intrusive dolerites (as well as the kimberlites) widely vary from the Ordovician to Early Carboniferous (496–321 Ma) (Tomshin et al., 2004). Geological data provoke doubts in some of the isotope dates. For example, the kimberlites of the Nyurba pipe (Nakyn field) contain xenoliths of sedimentary rocks with Ordovician, Silurian, and Middle Devonian fauna (Tarabukin et al., 2003), as well as xenoliths of dolerites (pre-kimberlite phase of basic rocks) and thin cross-cutting dikes of alkali potassium basic rocks. However, the isotope ages of kimberlites and basic rocks of the Nyurba pipe vary from the Middle Ordovician to Early Carboniferous (Agashev et al., 2004; Zaitsev et al., 2001; Mashchak and Naumov, 2004; Oleinikov, 1979; Tomshin et al., 1998, 2004; Agashev et al., 1998). This inconsistency requires more detailed geochronological studies.

PETROGRAPHY AND ISOTOPE GEOCHEMISTRY OF THE ROCKS

Petrographic characteristics. Subvolcanic rocks of the Vilyui–Markha dike belt are medium-grained subalkali basic rocks, dolerites, with ophitic, poikiloophitic, and taxtitoophitic textures. They have fairly uniform primary mineral assemblages. The major minerals are plagioclase (labradorite), clinopyroxene, olivine (no more than 5–10%), as well as accessory apatite, ilmenite, Ti-magnetite, and uncommon titanite. The late magmatic minerals are scarce biotite flakes in association with Ti-magnetite, as well as quartz–feldspar aggregates in olivine-free dolerites. Olivine is usually partially or completely replaced by talc–magnetite–serpentine or bowlingite pseudomorphs. Plagioclase is the most resistant to secondary alterations. Its grains are zonal and replaced by sericite, chlorite, and occasional alkali feldspar. Clinopyroxene is variably altered up to complete replacement by secondary minerals, for example, amphibole, which is, in turn, replaced by chlorite.

The composite dikes contain, in addition to dolerites, monzonite porphyries. These are fine-grained often porous rocks with large phenocrysts of tabular plagioclase up to 5 mm in size. The texture of the rock

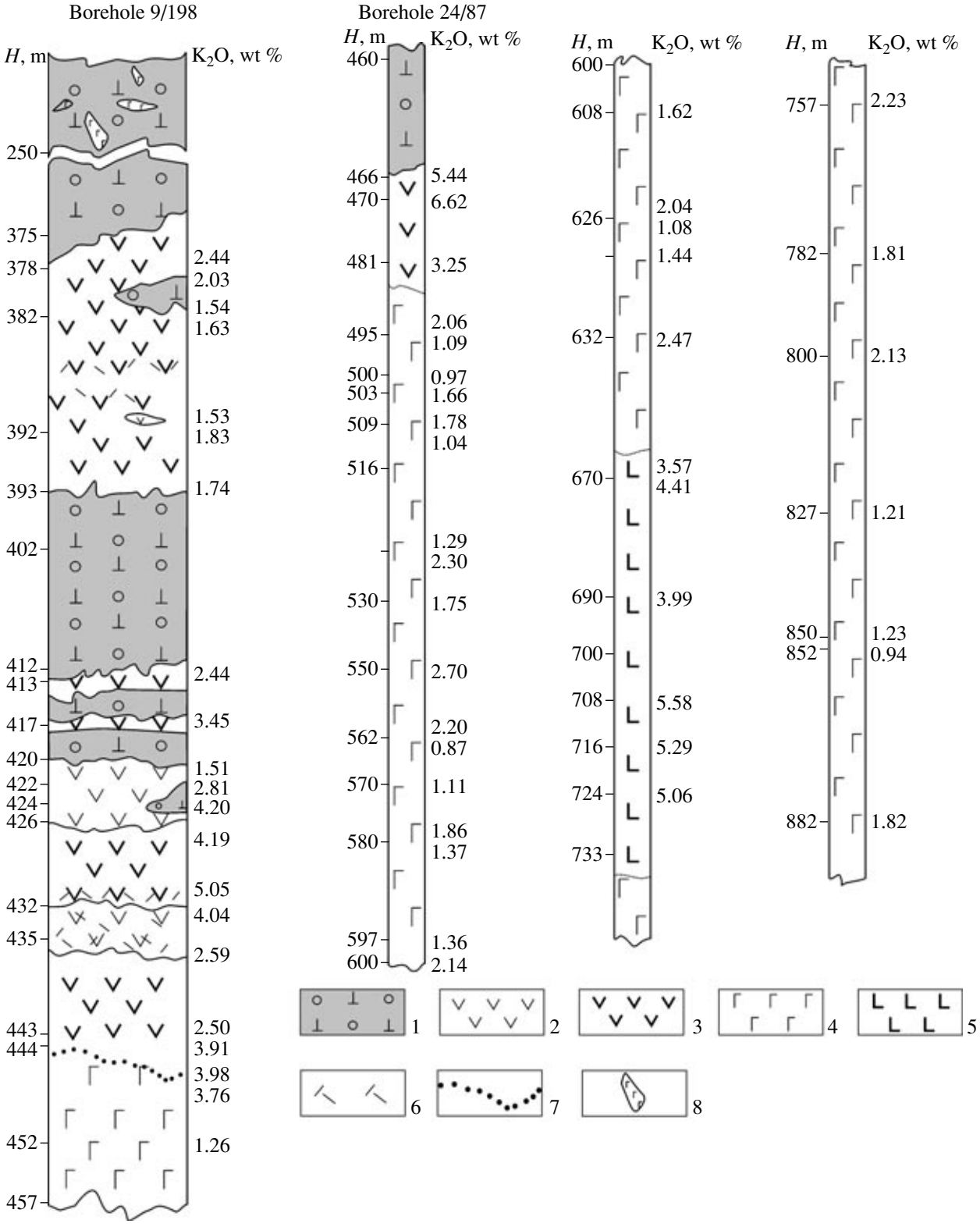

Fig. 2. Geological relations between kimberlites, alkali and subalkali basic rocks in the Nyurba pipe.

(1) Kimberlites (autolithic kimberlite breccia); (2, 3) dike and vein bodies of (2) alkali glassy microdolerites of hyalobasalt type and (3) microdolerites cutting across kimberlites; (4) pre-kimberlite subalkali medium-grained dolerites; (5) monzonite porphyries (final phase of the composite dike varying in composition from pre-kimberlite olivine-bearing dolerites to quartz-bearing dolerites and monzonite porphyries; character of contact (gradual or cross-cutting) between dolerites and monzonite porphyries was not established; (6) brecciated basalts; (7) contacts of unclear character; (8) xenoliths of subalkali dolerites in kimberlites. Numerals on the right-hand side of the borehole sections demonstrate the K distribution in the pre-kimberlite and post-kimberlite basalts, and the depth is indicated on the left-hand side (*H*, m).

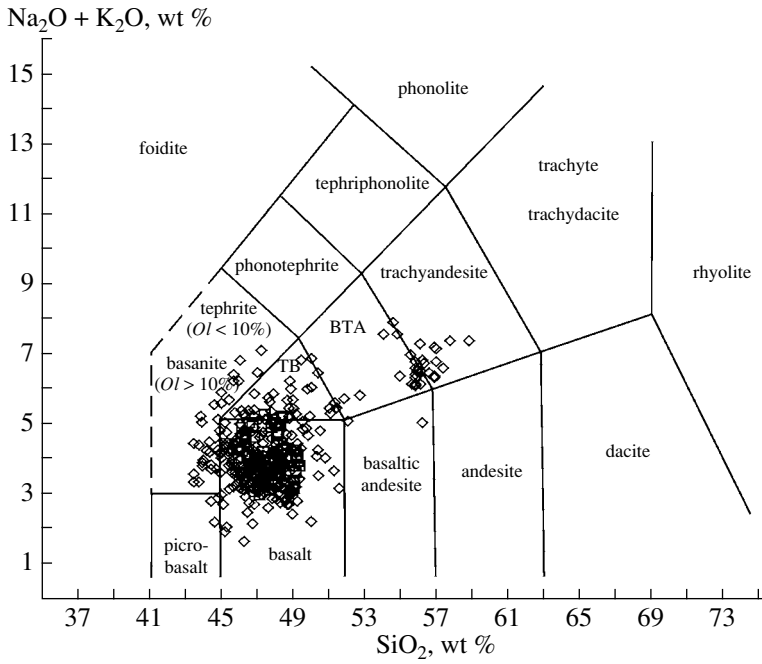

Fig. 3. Total alkalis versus silica in the Middle Paleozoic basalts of the Vilyui–Markha dike belt (original and reported data). (TB) trachybasalt, (BTA) basaltic trachyandesite.

is porphyritic and glomerophyric. Along with plagioclase (~20%), phenocrysts consist of clinopyroxene (≤7%). The groundmass is fine-grained fully crystalline with apographic and micropoikilitic patches. It consists of plagioclase, alkali feldspar (K_2O = 10.1–10.5 wt %, Na_2O = 2.6–3.3 wt %), hornblende, biotite (≤5%), quartz (<10%), Ti-magnetite, ilmenite, accessory apatite, and titanite. The secondary minerals are sericite, chlorite, and carbonate.

Within the Nakyn field, the basic rocks with alkali feldspar occur as dikes and veins cutting across kimberlites. Texturally, they correspond to hyalobasalts and microdolerites and consist of plagioclase, clinopyroxene, iron oxide, ilmenite, amphibole, and chlorite. The glassy matrix typically contains microphenocrysts of plagioclase, less common clinopyroxene, and ilmenite. Alkali feldspar is easily identified by microprobe analysis. It developed after plagioclase and typically did not form primary phenocrysts. Other K-bearing phases are the devitrification products of the intergranular matrix, which consists of a mixture of alkali feldspar, Ti-magnetite, and chlorite in variable proportions. Poenites (potassium spilites), which are enriched in potassium (up to 7 wt % K_2O) and strongly depleted in sodium (Na_2O < 1 wt %) occur in the areas of the most pervasive metasomatic alteration associated with the removal of Ca and Na and the input of K and Mg.

The volcanic covers associated with the dike belt are composed mainly of basalts. They show a massive, amygdaloidal structure and a porphyritic texture. The phenocrysts vary in size from a few tenths of a millimeter to 5–6 mm, accounting for no more than 5–8 vol %. They are made up of olivine (replaced by bowlingite pseudomorphs) and more often of single or glomerophyric intergrowths of plagioclase. The groundmass has a doleritic, intercertal, or, more rarely, a hyaline texture and consists of plagioclase, clinopyroxene, Ti-magnetite, ilmenite, and single biotite grains in association with Ti-magnetite and accessory apatite. The secondary minerals are chlorite, chlorite–serpentine, sericite, zeolite, carbonates, quartz, and chalcedony. In places, basalts experienced pervasive palagonitization.

Chemical composition. Petrogeochemical data (Table 1) characterize various facies of riftogenic magmatism: lavas (basalts of the Appain Formation) and subvolcanic (sills, dikes, including composite dikes with the participation of monzonite porphyries in contact with kimberlites of the Nyurba pipe). The SiO_2 content in the rocks varies from 44 to 49 wt %, increasing to 56 wt % only in the monzonite porphyries. In a ($Na_2O + K_2O$)–SiO_2 (Fig. 3) classification diagram, the bulk of the rocks correspond to basalts and, to a lesser extent, trachybasalts and tephrites. A separate cluster of monzonite porphyries plots in the field of basaltic trachyandesites and trachyandesites.

The basic rocks of the Vilyui rift are differentiated rocks (Mg# = 0.35–0.55). With increasing SiO_2, they demonstrate an increase in CaO and Al_2O_3 and a decrease in TiO_2, K_2O, P_2O_5, and FeO_{tot}. The MgO content varies mainly from 5 to 7 wt % and has no visible correlation with SiO_2 content. It should be noted that CaO shows positive correlation with Al_2O_3, indicating an important role of plagioclase fractionation in chemical variations of the rocks of the Vilyui rift. In

Table 1. Chemical composition of the basic rocks from northwestern Vilyui rift

Component	Pre-kimberlite dikes of the Vilyui–Markha belt							
	4/00	10/00	16b/00	v/16	8/00	41/01	43/01	74a
SiO_2	46.74	47.85	47.49	47.83	47.06	48.45	47.84	47
TiO_2	4.5	3.24	3.28	2.87	3.80	2.01	3.20	3.51
Al_2O_3	12.17	13.4	14.18	13.1	13.71	14.5	15.3	13.56
FeO*	15.77	13.41	14.55	16.01	14.20	11.15	12.15	14.91
MnO	0.3	0.16	0.2	0.36	0.23	0.2	0.2	0.61
MgO	5.28	5.61	4.91	5.29	5.09	6.61	4.83	5.48
CaO	8.77	10.2	9.64	9.23	9.35	11.0	9.26	8.17
Na_2O	2.04	2.18	2.39	2.14	2.31	2.1	2.21	2.38
K_2O	1.79	1.0	0.97	0.91	1.38	0.65	1.33	1.69
P_2O_5	0.4	0.3	0.35	0.29	0.28	0.2	0.32	0.42
L.O.I.	0.69	1.25	0.58	0.41	0.91	1.64	1.73	1.56
Total	98.45	98.60	98.54	98.44	99.89	100.26	100.17	99.81
Sc	31	32	34	26	38	42	40	331
V	346	306	294	246	405	348	368	93
Cr	17	147	70	23	64	109	209	46
Co	40	44	39	41	50	51	47	80
Ni	30	34	42	39	56	67	105	39
Rb	32	18	25	21	32	16	29	37
Sr	383	498	303	339	631	293	277	405
Y	37.6	30.7	38.0	30.0	32.6	27.7	41.5	43.1
Zr	268	201	256	181	161	160	279	183
Nb	29.7	26.9	36.0	21.9	33.3	19.7	39.9	38.6
Ba	275	167	229	290	218	197	258	331
La	42.6	32.2	48.7	28.9	24.9	17.7	30.0	30.9
Ce	89.8	68.8	91.9	60.1	55.2	41.0	68.1	71.8
Pr	9.7	7.9	10.2	7.2	6.7	5.4	8.6	8.6
Nd	39.2	31.6	40.1	28.7	31.0	24.2	37.3	39.8
Sm	7.88	6.57	7.59	6.22	7.28	5.73	8.27	8.82
Eu	2.34	2.08	2.32	1.85	2.25	1.77	2.43	2.52
Gd	7.59	6.69	8.11	6.46	7.1	5.54	8.72	9.44
Tb	1.24	1.08	1.3	1.03	1.04	0.92	1.38	1.59
Dy	7.26	5.85	7.58	5.9	5.97	5.23	7.82	8.38
Ho	1.47	1.22	1.63	1.18	1.2	1.06	1.6	1.69
Er	3.87	3.1	4.35	3.18	2.97	2.94	4.33	4.76
Tm	0.51	0.42	0.62	0.48	0.41	0.46	0.69	0.66
Yb	3.12	2.58	3.62	2.9	2.5	2.5	3.88	3.96
Lu	0.43	0.32	0.51	0.38	0.35	0.38	0.58	0.56
Hf	6.11	5.01	6.38	4.72	4.43	4.14	7.09	4.74
Ta	1.67	1.53	2.03	1.19	2.05	1.57	2.58	2.14
Pb	3.0	0.1	1.8	4.2	2.4	2.4	3.9	23.1
Th	3.34	2.2	3.1	2.06	2.14	2.02	3.67	3.04
U	0.88	0.61	0.89	0.65	0.61	0.62	0.98	0.85

Table 1. (Contd.)

Component	Basalts of the Appain Formation				Pre-kimberlite basalts of the Nyurba pipe				Monzonite porphyries of the Nyurba pipe	
	418/5b	420/32	427/2	420/54	12d-1	23/00	26/00	53-9	75b	53-1
SiO_2	48.26	49.14	48.34	48.78	46.2	48.78	46.25	45.04	52.72	55.56
TiO_2	2.57	2.54	2.53	2.34	4.69	2.12	4.83	5.20	3.14	2.61
Al_2O_3	14.23	14.11	14.38	14.41	13.62	13.45	13.04	12.4	12.55	13.25
FeO*	12.06	12.13	12.02	12.49	14.94	13.32	15.25	16.94	13.69	11.93
MnO	0.13	0.14	0.15	0.16	0.15	0.31	0.44	0.24	0.14	0.11
MgO	6.64	5.83	5.78	6.08	5.15	6.06	5.06	5.23	3.64	2.1
CaO	9.59	10.1	10.2	10.26	8.4	10.67	9.14	8.34	3.92	2.3
Na_2O	2.32	2.44	2.37	2.16	2.46	2.08	2.32	2.27	2.31	2.52
K_2O	0.81	0.79	0.84	0.71	1.26	0.69	0.97	0.94	3.51	4.41
P_2O_5	0.29	0.28	0.28	0.26	0.67	0.22	0.54	0.58	1.04	0.7
L.O.I.	1.79	1.01	1.65	0.95	2.33	0.92	0.6	1.84	2.62	2.99
Total	100.03	99.86	99.88	98.60	100.53	98.62	100.13	100.39	99.92	99.21
Sc	42	42	41	27	400	36	33	479	199	181
V	368	375	373	240	39	219	412	55	28	16
Cr	176	172	170	62	43	45	43	56	30	28
Co	48	46	45	40	53	48	39	68	31	21
Ni	76	75	71	42	36	43	44	43	26	23
Rb	21	19	20	14	17	15	26	32	136	147
Sr	397	381	384	318	622	233	481	297	332	366
Y	28.3	29.1	29.4	22.8	62.9	25.7	61.6	63.9	99.4	90.4
Zr	192	335	180	139	433	140	356	505	225	226
Nb	23.4	22.6	23.0	16.4	60.1	17.0	51.7	63.7	95.1	84.4
Ba	241	284	267	192	215	206	156	198	537	599
La	20.4	21.1	19.4	24.1	40.3	24.5	47.1	43.6	129.4	128.6
Ce	46.7	48.8	46.5	49.9	100.1	51.3	104.6	103.0	286.4	271.3
Pr	6.2	6.4	5.9	5.8	12.3	5.8	12.4	12.6	32.3	29.9
Nd	27.4	28.0	26.3	22.3	59.6	23.5	58.9	60.0	139.6	128.7
Sm	6.35	6.56	6.06	4.61	13.3	4.87	13.57	13.76	27.47	24.05
Eu	2.13	2.16	1.97	1.44	3.6	1.44	3.53	3.72	6.09	5.69
Gd	6.05	6.32	5.89	4.67	13.99	4.95	12.97	14.44	25.14	22.56
Tb	0.93	0.99	0.95	0.75	2.25	0.83	2.07	2.27	3.85	3.46
Dy	5.42	5.54	5.13	4.28	12.33	4.77	11.3	12.19	19.89	17.72
Ho	1.04	1.08	1.03	0.89	2.37	0.99	2.36	2.48	3.74	3.39
Er	2.72	2.94	2.96	2.32	6.54	2.81	5.78	6.69	10.24	8.88
Tm	0.43	0.46	0.46	0.32	0.92	0.38	0.82	0.93	1.38	1.28
Yb	2.29	2.71	2.34	1.9	5.01	2.51	4.79	5.18	7.36	6.9
Lu	0.36	0.4	0.36	0.25	0.76	0.36	0.68	0.74	1.1	0.97
Hf	4.64	8.24	4.36	3.35	10.5	3.49	9.59	12.09	7.86	8.02
Ta	1.52	1.48	1.57	0.98	3.43	1.01	3.3	3.47	5.87	5.38
Pb	2.0	2.5	1.9	0.1	0.1	1.0	2.1	0.8	4.3	3.8
Th	2.1	2.26	2.1	1.31	4.82	1.65	4.63	4.58	20.62	22.79
U	0.57	0.64	0.53	0.39	1.35	0.52	1.38	1.37	5.68	5.94

Table 1. (Contd.)

Component	Sills of the Nakyn field				Post-kimberlite basalts of the Nyurba pipe				
	2cm-701	2cm-671	2cm-715	2cm-669	12g-2	12d	12/00	12g-1	22/00
SiO_2	48.01	48.16	47.62	47.92	46.83	46.32	44.7	45.01	46.51
TiO_2	2.87	3.17	3.17	2.66	4.87	4.71	5.45	4.95	4.93
Al_2O_3	12.58	12.98	13.62	13.78	12.01	12.35	12.98	11.62	11.94
FeO*	15.80	16.06	15.25	15.19	11.75	15.41	15.14	14.62	16.04
MnO	0.21	0.2	0.18	0.2	0.15	0.19	0.1	0.13	0.3
MgO	5.55	5.26	5.35	5.17	7.09	5.58	6.86	6.6	5.83
CaO	9.58	8.83	8.52	9.8	7.88	6.22	5.47	6.62	7.14
Na_2O	2.41	2.28	2.38	2.43	1.35	1.51	2.28	0.84	2.03
K_2O	0.98	0.93	1.15	0.9	4.04	3.92	2.44	5.05	1.54
P_2O_5	0.3	0.32	0.32	0.3	0.7	0.62	0.77	0.69	0.72
L.O.I.	1.5	1.72	2.1	1.75	1.74	1.2	2.05	1.82	1.36
Total	100.47	100.40	100.11	100.47	99.62	99.75	99.93	99.3	98.34
Sc	407	369	372	34	38	36	40	38	20
V	103	68	66	89	421	425	462	438	273
Cr	55	50	54	50	100	57	112	149	24
Co	71	65	64	61	22	44	42	34	33
Ni	43	40	41	38	43	51	64	56	25
Rb	21	25	28	21	54	61	39	46	31
Sr	330	296	389	332	2718	849	364	3452	268
Y	39.9	41.3	41.9	37.5	65.4	62.9	61.1	72.2	53.7
Zr	185	242	207	180	420	403	508	432	402
Nb	28.4	31.2	31.7	26.8	62.9	61.6	68.0	61.9	38.6
Ba	230	165	395	329	165	190	230	117	256
La	24.0	25.7	26.3	23.7	38.2	47.1	56.4	49.9	57.4
Ce	53.4	56.0	57.9	51.6	89.9	105.7	127.0	114.3	123.2
Pr	6.7	7.2	7.2	6.7	10.9	12.4	15.2	13.8	14.6
Nd	30.0	31.3	32.4	29.4	52.6	59.5	73.0	66.5	59.7
Sm	7.47	7.61	7.77	7.25	12.67	14.12	16.67	15.8	12.78
Eu	2.20	2.22	2.13	2.15	2.07	3.47	4.17	2.91	3.23
Gd	7.63	7.69	8.09	7.30	12.59	13.28	15.24	14.87	12.42
Tb	1.20	1.19	1.25	1.16	2.02	2.12	2.29	2.44	2.01
Dy	6.55	6.51	6.83	6.35	11.61	11.6	12.55	13.16	11.73
Ho	1.31	1.29	1.37	1.27	2.45	2.32	2.48	2.68	2.35
Er	3.46	3.50	3.57	3.29	5.89	5.75	6.03	6.54	5.66
Tm	0.55	0.55	0.57	0.51	0.87	0.84	0.92	0.98	0.9
Yb	3.26	3.24	3.42	3.15	5.24	4.96	5.54	5.7	4.94
Lu	0.48	0.49	0.51	0.46	0.74	0.69	0.76	0.8	0.71
Hf	4.16	5.55	5.07	3.99	11.13	10.78	13.34	11.81	10.49
Ta	1.32	1.42	1.44	1.22	3.82	4.19	4.17	3.87	2.25
Pb	2.6	2.3	1.1	2.6	1.2	1.2	8.7	1.4	0.1
Th	2.13	2.16	2.25	1.98	5.65	5.52	6.2	5.59	4.22
U	0.68	0.72	0.74	0.67	1.69	1.42	1.93	1.65	1.22

Table 1. (Contd.)

Component	Post-kimberlite basalts of the Nyurba pipe								
	12b	2g/00	64a	61	62a	64	65b	65v	65a
SiO_2	46.7	46.47	42.02	41.01	44.45	44.43	44.61	46.78	45.58
TiO_2	4.88	4.77	5.38	4.21	5.22	5.01	5.38	5.12	5.46
Al_2O_3	11.7	13.29	14	11.14	13.4	13.3	12.53	14	12.86
FeO*	16.11	12.88	15.89	9.51	16.25	15.86	17.51	16.19	16.77
MnO	0.16	0.13	0.11	0.02	0.09	0.15	0.19	0.04	0.12
MgO	5.66	6.35	6.22	9.04	5.97	6.17	5.19	4.86	4.81
CaO	7.71	9.12	4.55	11.26	6.45	6.89	6.63	3.79	6.78
Na_2O	2.15	2.21	1.95	0.57	2.36	2.18	1.35	1.29	1.92
K_2O	1.54	1.67	1.74	3.45	1.51	1.53	4.19	2.81	2.59
P_2O_5	0.7	0.51	0.67	0.72	0.72	0.71	0.64	0.71	0.76
L.O.I.	1.02	0.93	3.47	4.18	2.52	3.11	1.57	3.39	2.07
Total	100.11	98.33	100.27	100.4	100.01	100.4	100.52	99.64	100.45
Sc	34	23	438	366	480	424	437	423	431
V	396	276	44	52	71	44	58	62	43
Cr	60	42	39	31	50	51	51	35	46
Co	43	43	47	57	66	54	60	61	52
Ni	52	53	40	34	44	38	38	38	40
Rb	38	36	43	40	39	39	62	25	30
Sr	353	561	350	237	410	357	1142	287	519
Y	62.3	27.5	52.2	60.0	67.3	61.2	63.6	63.3	74.3
Zr	297	264	315	350	503	348	457	459	600
Nb	56.7	35.6	66.3	53.9	70.7	63.7	64.2	62.1	76.0
Ba	263	309	208	223	225	188	192	258	131
La	50.5	46.6	48.8	51.7	49.4	47.0	45.3	48.7	50.1
Ce	112.2	100.1	113.0	119.5	117.8	111.3	107.2	112.1	125.8
Pr	13.4	11.6	13.7	14.4	14.3	13.7	13.2	13.3	15.5
Nd	64.6	45.9	62.4	66.9	67.7	64.0	62.3	62.0	72.8
Sm	14.71	9	13.44	14.68	15.11	13.7	14.81	13.91	16.32
Eu	3.76	2.69	3.76	4.04	4.01	3.8	3.82	3.28	4.17
Gd	13.86	7.84	13.04	14.79	15.61	14.59	14.85	14.7	17.26
Tb	2.21	1.18	2.11	2.32	2.5	2.21	2.34	2.33	2.72
Dy	11.86	6	11	12.37	13.89	12.33	12.64	12.55	14.52
Ho	2.39	1.04	2.13	2.25	2.71	2.37	2.45	2.46	2.87
Er	5.93	2.63	5.83	6.08	7.44	6.3	6.87	6.86	7.97
Tm	0.82	0.35	0.78	0.83	1.06	0.85	0.94	0.97	1.05
Yb	4.8	1.99	4.44	4.76	5.78	4.68	5.38	5.39	6.2
Lu	0.65	0.25	0.63	0.64	0.87	0.69	0.73	0.76	0.83
Hf	8.04	6.07	8.4	8.93	12.67	8.71	11.2	11.73	14.83
Ta	3.61	2	3.87	3.05	4.22	3.62	3.72	3.53	4.24
Pb	1.3	0.8	0.3	0.5	3.9	2.4	0.2	0.5	1.0
Th	3.48	3.74	3.45	4.14	5.32	3.47	4.67	4.84	5.25
U	0.95	0.99	0.94	1.3	1.58	0.97	1.35	1.4	1.66

Note: Analysis of trace elements was performed on a PlasmaQuad 3 VG Elemental ICP-MS mass spectrometer. Silicate analysis was conducted at the Vinogradov Institute of Geochemistry and Analytical Chemistry, Siberian Division, Russian Academy of Sciences. Major elements are given in wt %, trace elements, in ppm.

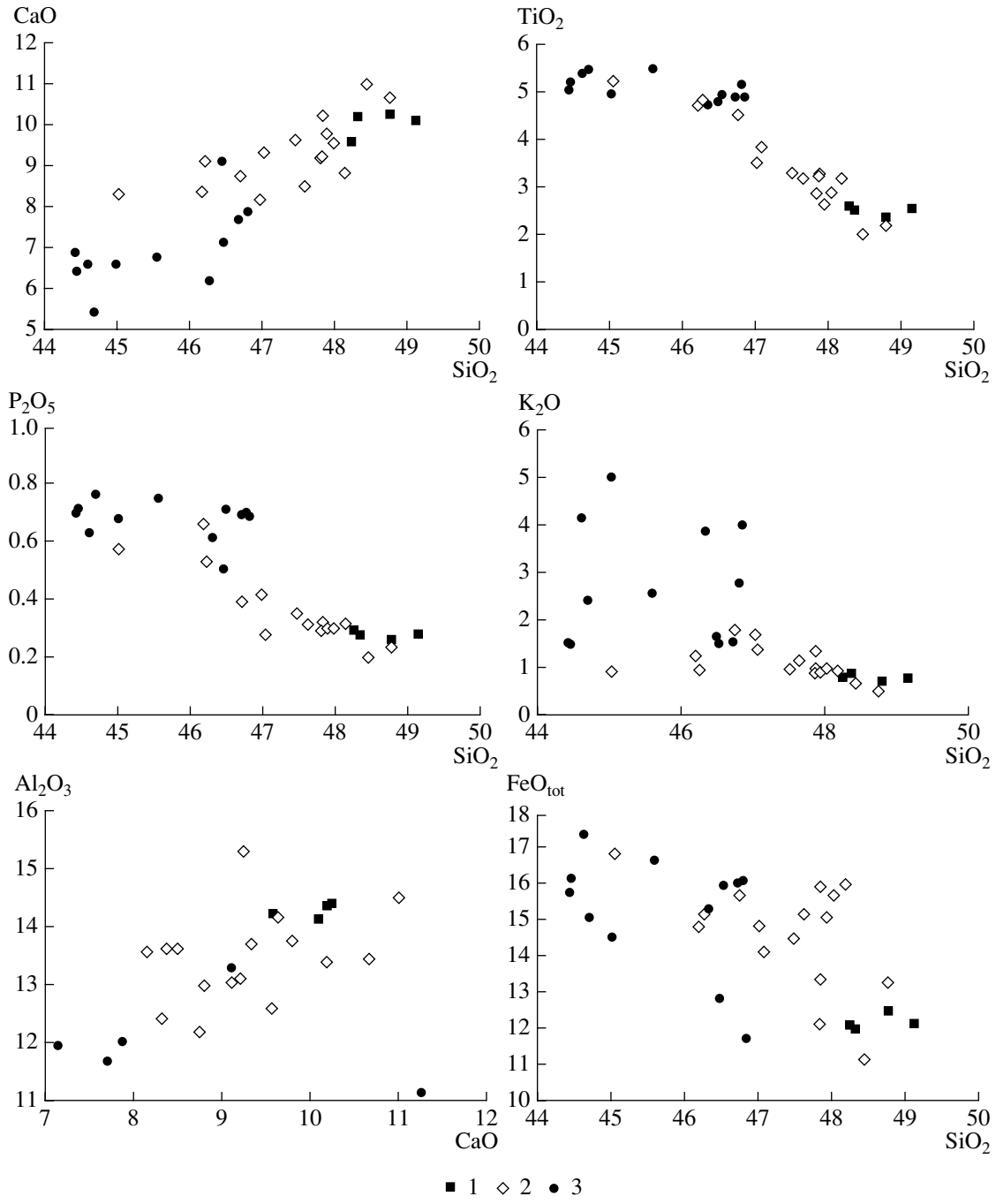

Fig. 4. Variations of major oxides (wt %) in the basic rocks of the Vilyui rift.
(1) Basalts of the Appain Formation, (2) subalkali dolerites of pre-kimberlite dikes and sills, (3) alkali potassium basalts of post-kimberlite dikes.

variation diagrams (Fig. 4), the data points of the rocks form a trend defined, in particular, by systematic compositional differences between rocks of different facies. For example, high contents of SiO_2 (48–49 wt %) and CaO and relatively low contents of TiO_2, K_2O, P_2O_5, and FeO_{tot} are typical of basaltic lavas. The subalkali dolerites that compose the pre-kimberlite dikes and sills occupy intermediate position between the lavas and the rocks of the post-kimberlite dikes. The latter have the lowest SiO_2 (up to 44 wt %) and CaO contents and the highest TiO_2, P_2O_5, FeO_{tot}, and K_2O. It should be noted that post-kimberlite basic rocks are somewhat depleted in Na and Si relative to the pre-kimberlite dolerites and enriched in K (~4–5 wt % K_2O) with respect to them. The rocks of all three groups contain norma-

tive olivine or, more rarely, normative nepheline and quartz.

The characteristic feature of the rift magmatic rocks is their derivation from high-Ti mantle melts. Low-Ti basic rocks are nearly absent, which strongly differentiates the magmatic association of the Vilyui rift from the flood basalts of Gondwana (Hawkesworh et al., 1984). The sampling (more than 300 analyses) can be grouped into moderate-Ti (<3 wt % TiO_2) and high-Ti (>3 wt % TiO_2) basaltic associations. The moderate-Ti group includes basic volcanic rocks of the Appain Formation (1.5–3 wt % TiO_2), as well as the sills of the Mirninskoe (1.8–2.8 wt % TiO_2) and Nakyn (1.9–2.6 wt %) kimberlite fields; the high-Ti group includes numerous dikes and fissure intrusions of subalkali dolerites (3.2–4.5 wt % TiO_2) and all studied post-kimberlite dikes of alkali potassium basalts (4.0–5.5 wt % TiO_2). The identified geological relations indicate that the moderate-Ti intrusive basic rocks were formed during the initial stage, while the high-Ti were produced during the final stage of the evolution of Middle Paleozoic basic magmatism. The moderate-Ti basalts occur mainly in rift depressions, the areas of maximum lithospheric extension and thinning, whereas the high-Ti basalts developed on the northwestern shoulder of the rift, within the thickened cratonal lithosphere. Following (Arndt and Christensen, 1992), these differences can be related to the different conditions of melting under the weakly ruptured cratonal lithosphere (low degree of melting) and beneath the thinner and broken lithosphere of the Vilyui Rift (higher degree of melting).

The **geochemical characteristics** of the rocks are shown in Table 1 and Figs. 5, 6. Let us consider the contents of some indicator elements occupying different position in the incompatibility sequence according to (Sun and McDonough, 1989). The elevated contents of Ni (70–75 ppm) and Cr (170–175 ppm) are typical of the basalts of the Appain Formation (Table 1). The subalkali dolerites of dike series show wide variations in these elements (55–100 ppm Ni, and 55–205 ppm Cr). The pre- and post-kimberlite dikes of the Nyurba pipe exhibit no significant differences in Ni and Cr contents, which are somewhat lower than those in the basalts of the Appain Formation and subalkali dolerites located beyond the Nyurba pipe. The lowest contents of these elements were found in the monzonite porphyries (high-Si derivatives of basaltic melt).

Most incompatible elements display a positive correlation with one another and with TiO_2, P_2O_5, K_2O, and Fe but a negative correlation with the SiO_2 content (Fig. 5), which possibly highlights the different degrees of melting during the formation of their parent magmas. In addition, there is a negative correlation between incompatible elements and CaO and Al_2O_3, which suggests a significant role of plagioclase fractionation in rock formation. The incompatible element ratios (Nb/Ta, Zr/Nb, La/Nb, Ta/Yb, Th/Ta, and others) vary within narrow ranges and remain practically unchanged over the entire SiO_2 range. The exceptions are the monzonites of the composite dikes, the strongly differentiated varieties of the rocks with correspondingly modified ratios of incompatible elements. These characteristics testify to either the leading role of fractionation in the evolution of parent magma or the relative homogeneity of the magma source, if the melt was controlled by variations in the degree of melting of this source.

The general relations in the distribution of incompatible elements in the rocks of the Vilyui rift are shown in spidergrams (Fig. 6). The trace-element patterns normalized to the primitive mantle (Sun and McDonough, 1989) are nearly identical, regardless of their position in the rift zone. The rocks of various facies differ mainly in the degree of enrichment in incompatible elements, with this degree increasing from the basalts of the Appain Formation to the pre-kimberlite subalkali dolerites and alkali potassium basalts of post-kimberlite dikes, in which only the contents of Ba and Sr remain unchanged. The monzonite porphyries of the composite dikes are distinguished from other rocks in having the highest contents of REE, Th, and U. At the same time, they have relatively low contents of Ba, Sr, and HFSE (Zr, Hf, Nb, Ta), which presumably signify the fractionation of plagioclase and Ti-bearing minerals.

The basalts of the Vilyui rift are similar to ocean island basalts (OIB), including the absence of a Ta–Nb minimum, which is characteristic of within-plate magmatic sources. However, the Vilyui basalts are more enriched in HREE relative to LREE (La/Yb = 10–18) than OIB, which possibly indicates the melting of a garnet-bearing source.

The **Nd and Sr isotopic compositions** of the considered rocks are shown in Table 2. The rocks are characterized by positive values of $\varepsilon_{Nd}(T)$ and $\varepsilon_{Sr}(T)$. In the diagram (Fig. 7), the data points plot above the mantle array and form three clusters in the mixing hyperbole with a concave upward curvature: (1) moderate-Ti rocks with the lowest ε_{Sr} (3.5–6.5) and relatively low ε_{Nd} (1.7–2.8); (2) high-Ti basic rocks with high ε_{Sr} (22–29); (3) high-Ti rocks with ε_{Nd} (3.5–5.5) higher than in the first cluster and ε_{Sr} (6.5–9) lower than in the second cluster. The data points of basalts in Fig. 7 are considered in the scope of a mixing model of sources depleted and enriched in radiogenic Sr (Kiselev et al., 2004).

GENESIS AND SOURCES OF THE BASALTS OF THE VILYUI RIFT

The geochemical and isotope–geochemical data presented above indicate that compositional variations in the magmatic rocks of the Vilyui rift were defined by different processes, including crystallization differentiation, contamination, different-scale melting, and the compositional heterogeneity of magma sources. It is

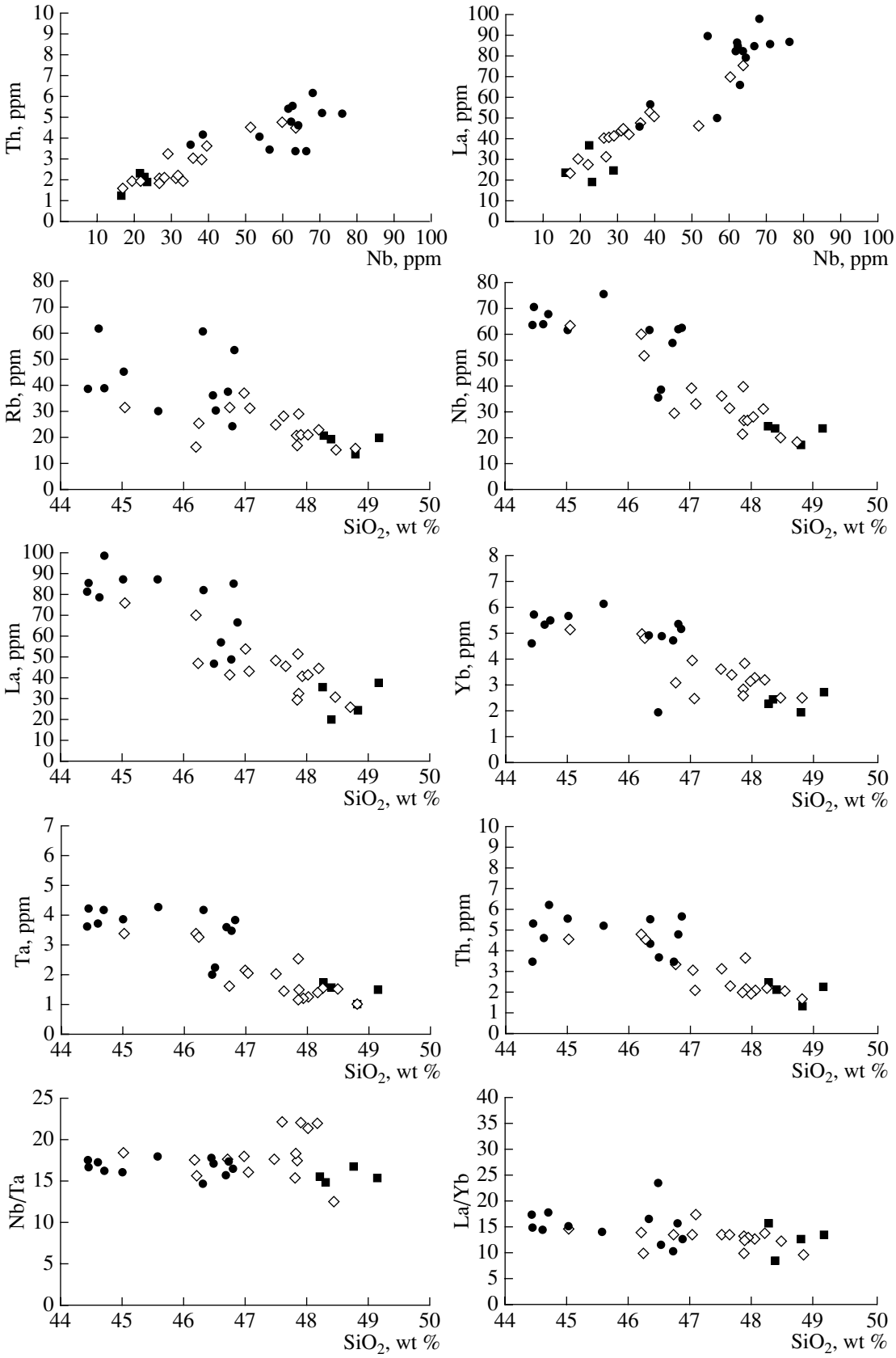

Fig. 5. Correlation of incompatible elements and their ratios with SiO_2 and each other. Symbols are as in Fig. 4.

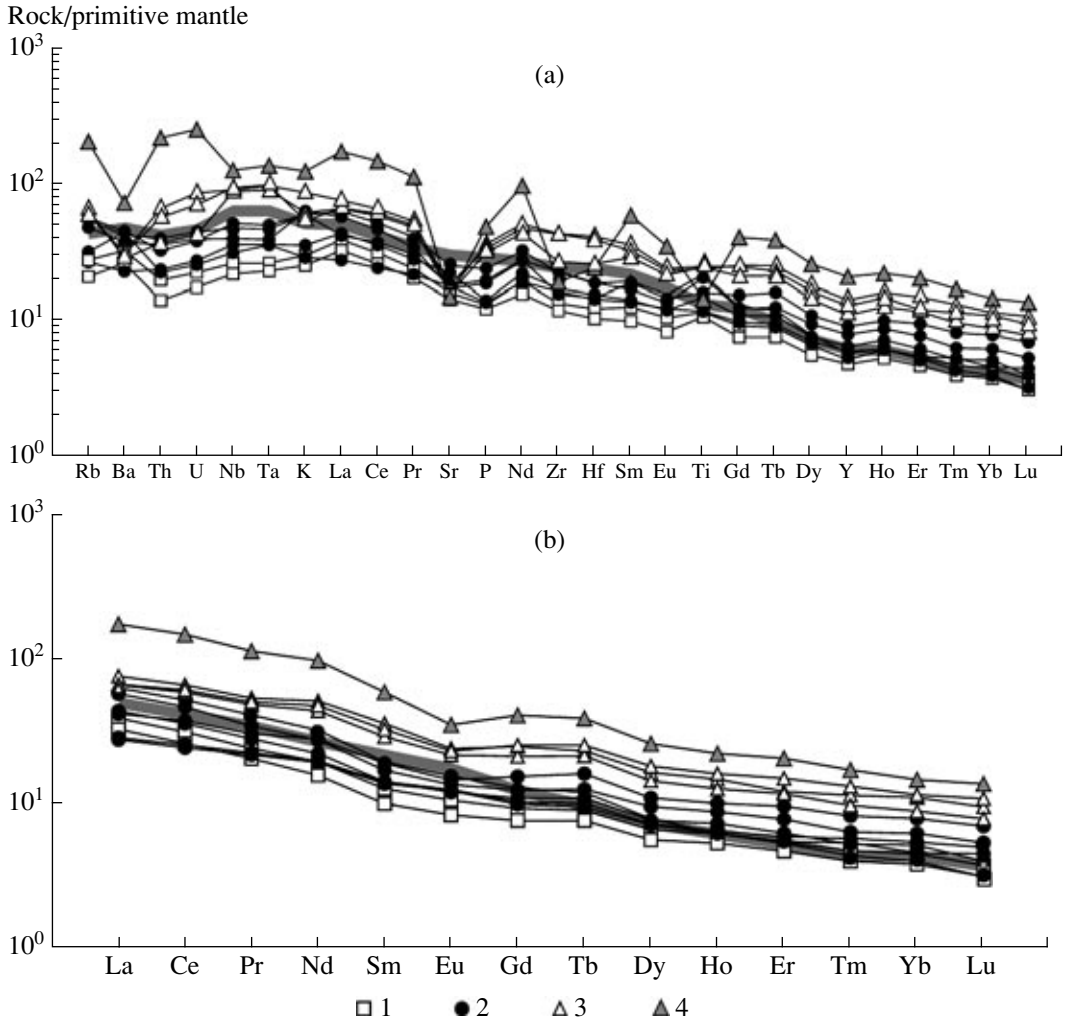

Fig. 6. Incompatible (a) and rare-earth element (b) distribution patterns for representative samples of the basic rocks. Normalizing values to primitive mantle were taken from (Sun and McDonough, 1989).

(1) Basalts of the Appain Formation, (2) subalkali dolerites of dikes and sills of pre-kimberlite intrusions, (3) alkaline potassium basalts of post-kimberlite dikes, (4) monzonites of complex dikes; Pattern for OIB is shown for comparison.

interesting to consider the role of these factors in the formation of the basalts of the Vilyui rift.

Crustal contamination. The presence of porphyroblasts of plagioclase, clinopyroxene, and olivine in the basalts and porphyroclasts of corroded plagioclase in the dolerites suggests that the melts resided for some time in magmatic chambers, crustal inclusive, and experienced both fractional crystallization and interaction with the wall rocks before eruption. The possibility of these processes can be estimated from the variations of Th, Ta, and Yb contents in the basalts. Crustal contamination brings about enrichment in Th relative to Ta and Yb, which is expressed, for example, in the increase of Th/Yb ratio (Pearce, 1983). In Fig. 8a, the data points of the basaltic rocks of the Vilyui rift plot slightly above the N-MORB–WPB field (Pearce, 1983). The relative enrichment of the rocks in Th can be caused by crustal contamination.

Given that incompatible element ratios remain constant over the entire compositional range of the rocks and differ from the crustal values, crustal contamination presumably played no significant role in the magmatic evolution of the Vilyui rift. In particular, the upper and lower crustal rocks have low Ce/Pb ratios (<5) and relatively high La/Nb ratios (~1.5 and 4.5, respectively) (Taylor and MacLennan, 1988), whereas the rift rocks have Ce/Pb > 10 and La/Nb < 1.5. Figure 8b demonstrates that compositional variations of the rift and crustal rocks are orthogonal, excluding notable crustal influence on the melts. A similar situation is seen in the Zr/La–Th/Ta diagram (Fig. 8c), which also demonstrates strong differences in the composition of the crust and considered magmatic rocks and the absence of any significant crustal influence on the latter.

Fractional crystallization. There is no doubt about the importance of fractionation in the evolution of mag-

Table 2. Nd and Sr isotope composition of the basalts of the Vilyui–Markha dike belt in the Nakyn kimberlite field

Sample No.	Rb, ppm	Sr, ppm	$^{87}Rb/^{86}Sr$	$^{87}Sr/^{86}Sr$	$^{87}Sr/^{86}Sr$*	$\varepsilon_{Sr}(T)$*	Sm, ppm	Nd, ppm	$^{147}Sm/^{144}Nd$	$^{143}Nd/^{144}Nd$	$\varepsilon_{Nd}(T)$*
10/00	19	600	0.09	0.70625	0.70573	24.0	7.3	32	0.14025	0.512672	3.5
V/16	26	440	0.17	0.70658	0.70562	22.5	7.1	31	0.13997	0.512645	3.0
16b/00	31	356	0.25	0.70590	0.70452	6.8	8.3	37	0.13759	0.512668	3.5
4/00	39	523	0.22	0.70706	0.70586	25.8	9.3	42	0.13496	0.512659	3.5
427/2	22	450	0.14	0.70529	0.70451	6.6	6.3	28	0.13731	0.512576	1.8
420/54	19	452	0.12	0.70504	0.70437	4.6	6.2	27	0.13966	0.512604	2.2
26/00	20	520	0.11	0.70625	0.70564	22.7	12.0	52	0.13966	0.512751	5.1
23/00	18	309	0.17	0.70525	0.70429	3.5	5.4	23	0.13955	0.512634	2.8
2g/00	45	758	0.17	0.70702	0.70606	28.6	10.0	49	0.12911	0.512530	1.3
22/00	43	375	0.33	0.70649	0.70467	8.9	15.0	64	0.13932	0.512763	5.3
12b/00	41	380	0.31	0.70625	0.70452	6.7	14.0	63	0.13981	0.512736	4.8

Note: Nd and Sr isotope analysis was conducted by D. Z. Zhuravlev on a Finnigan MAT-262 multicollector mass spectrometer in static mode, using the standard method (Zhuravlev et al., 1983).
* Values were calculated for an age of 300 Ma.

matic melts of the Vilyui rift. This follows from the low Mg# (0.35–0.55), relatively low contents of Ni (40–80 ppm) and Cr (30–200 ppm), as well as correlations between incompatible elements, which are consistent with their derivation through fractional differentiation. Dominant fractionation of olivine is suggested for the early stage of the magmatic evolution, bringing about a decrease in the MgO content of the rocks up to 5 wt % and, correspondingly, Mg# up to 0.55–0.35. During later stages, olivine fractionation gave way to fractionation of plagioclase, clinopyroxene and ore minerals, including accessory apatite, ilmenite, and Ti-magnetite, which formed phenocrysts. The correlation between SiO_2, CaO, and Al_2O_3 indicates that both the fractionation of plagioclase and its accumulation played a significant role in generating the compositional variations of the melt. In particular, assuming ~47% SiO_2 in the parental melt, the rocks with SiO_2 ~49 wt % could be obtained by the floatation and accumulation of ~30 wt % plagioclase, while rocks with SiO_2 content of ~45 wt % could be produced by the fractionation of about 25 wt % of the mineral (the composition of plagioclase typical of subalkali basalts was taken as model (wt %): SiO_2 53, CaO 13, Al_2O_3 28, Na_2O 5). This model satisfacto-

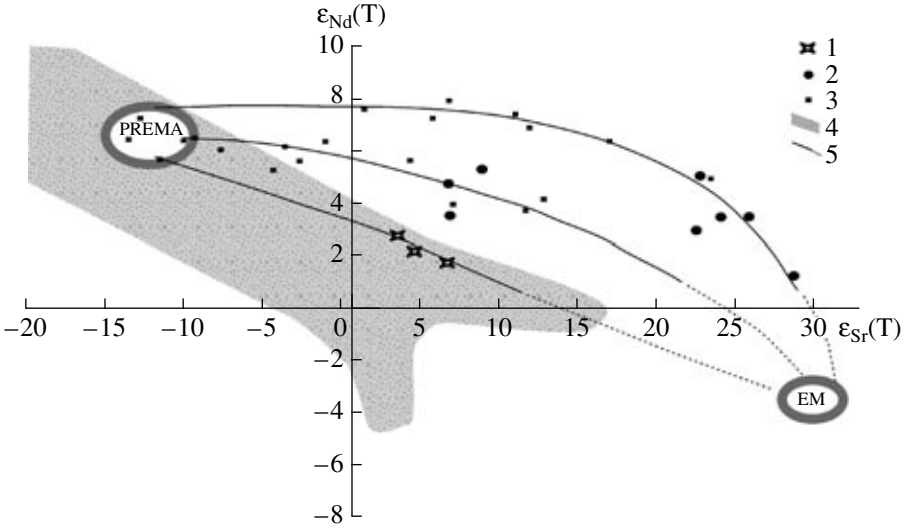

Fig. 7. ε_{Nd}–ε_{Sr} diagram for basalts of the northwestern shoulder of the Vilyui paleorift.
(1) Moderate-Ti basalts, (2) high-Ti basalts, (3) riftogenic basalts of the Altai–Sayan area after (Yarmolyuk and Kovalenko, 2003), (4) compositional field of mantle rocks (mantle array), (5) mixing hyperboles corresponding to high Sr/Nd ratio and varying Sr content in EM source. Mantle sources: PREMA is moderately depleted mantle, EM is the mantle enriched in radiogenic Sr.

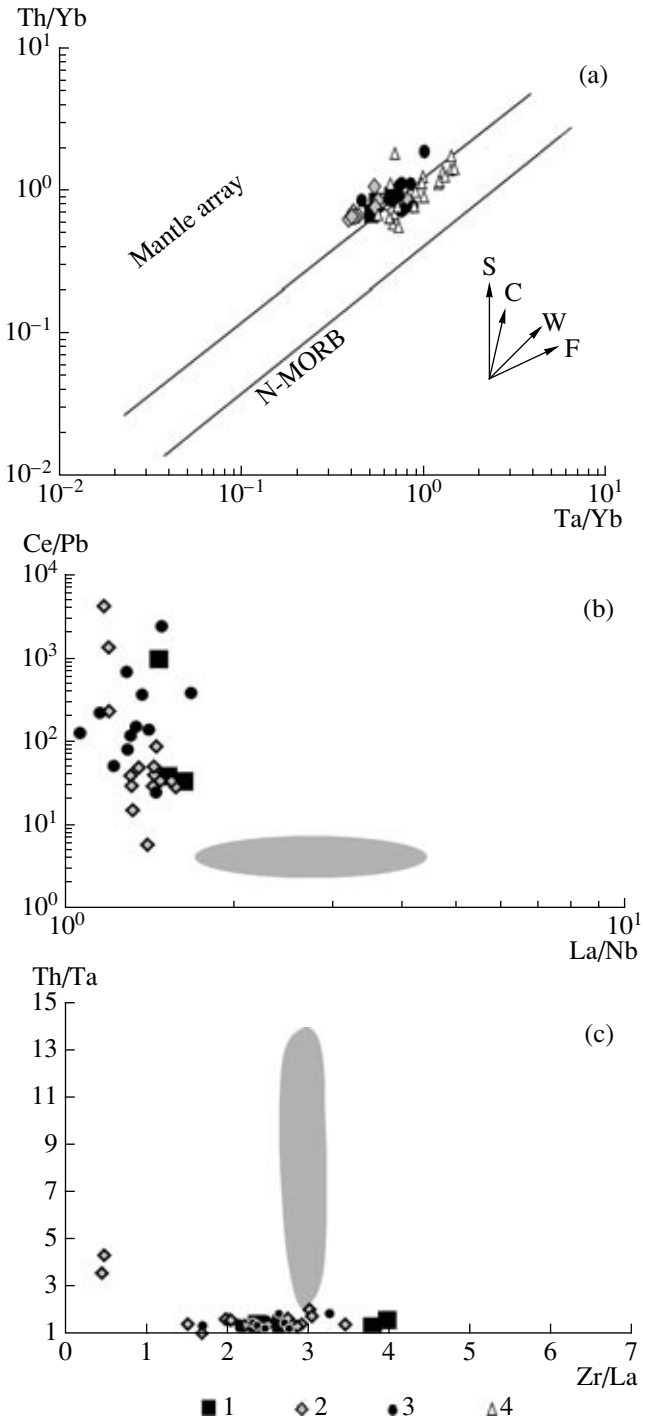

Fig. 8. Basalts of the Vilyui rift in correlation diagrams for incompatible elements.

Vectors: (S) subduction enrichment, (C) crustal contamination, (W) within-plate enrichment, (F) fractional crystallization. Symbols (1–3) are as in Fig. 4, (4) are basic rocks of the rift zones of the Altai–Sayan area. The gray field is the continental crust after (Gao et al., 1998).

rily describes the distribution of incompatible elements, in particular, explains the appearance of the negative Eu anomaly (Fig. 6) in the alkali basalts of low-Si post-kimberlite dikes. Nonetheless, it cannot explain the isotopic variations, the comparatively low Al_2O_3 contents in the rocks, the low abundance of plagioclase phenocrysts (<10%) in the highest-SiO_2 (up to 49 wt %) basalts of the Appain Formation, and the observed range of incompatible elements.

However, olivine–clinopyroxene–plagioclase fractionation presumably was one of the leading mechanisms in the crystallization differentiation of the basaltic magmas of the Vilyui rift. Rare monzonite porphyries of the late stage were formed owing to change from clinopyroxene–plagioclase to amphibole–plagioclase (±oxides, apatite) fractionation. Under deep-seated conditions, prograde crystallization was accompanied by an increase in the water content in the residual melts and by the appearance of amphibole and, to a lesser extent, biotite.

The composite dike 50–70 m thick at the contact with kimberlites of the Nyurba pipe is of interest from the genetical viewpoint. The change of rock composition from near-contact olivine-bearing dolerites through quartz-bearing dolerites to monzonite porphyries in the dike core at the absence of sharp contacts suggests two mechanisms of dike formation: (1) the involvement of compositionally different batches of fractionating melt in the intrusive process; (2) postinjection fractionation within the dike. The latter mechanism is less probable, because it can act only in thick dikes, through the successive movement of residual liquid from the crystallization zone of the marginal part of the dike toward its fused (liquid) center (Langmuir, 1989).

Source heterogeneity and formation conditions of the melt. Variations in the melting conditions and source heterogeneity of the melts follow, first of all, from petrogeochemical data: the predominance of high-Ti basalts enriched in incompatible elements within cratonal structures surrounding the Vilyui rift and the development of moderate-Ti basalts with relatively high SiO_2 content in the rift depressions. In accordance to geochemical data, the basaltic melts were derived from a garnet-bearing mantle source. To determine the melting conditions, we used data on the distribution of incompatible elements in the melts that arose during the melting of mantle peridotite with variable garnet content (MacDonald et al., 2001; Rogers et al., 2000). Figure 9 portrays the compositional variations with a change in the degree of melting (up to 3%) and garnet content (up to 8%) in the mantle source. Judging from the distribution of the data points, the rocks of the Vilyui rift were derived from garnet peridotites with garnet contents of up to 8%, averaging 4%. The degree of melting varied from 1.5 to 3%. In Fig. 9, the rock compositions are subdivided into moderate-Ti ($TiO_2 < 3$ wt %) and high-Ti ($TiO_2 > 3$ wt %). As follows from the plot, the melts of both rock groups were formed within the same depth interval from compositionally similar sources, but the moderate-Ti basalts

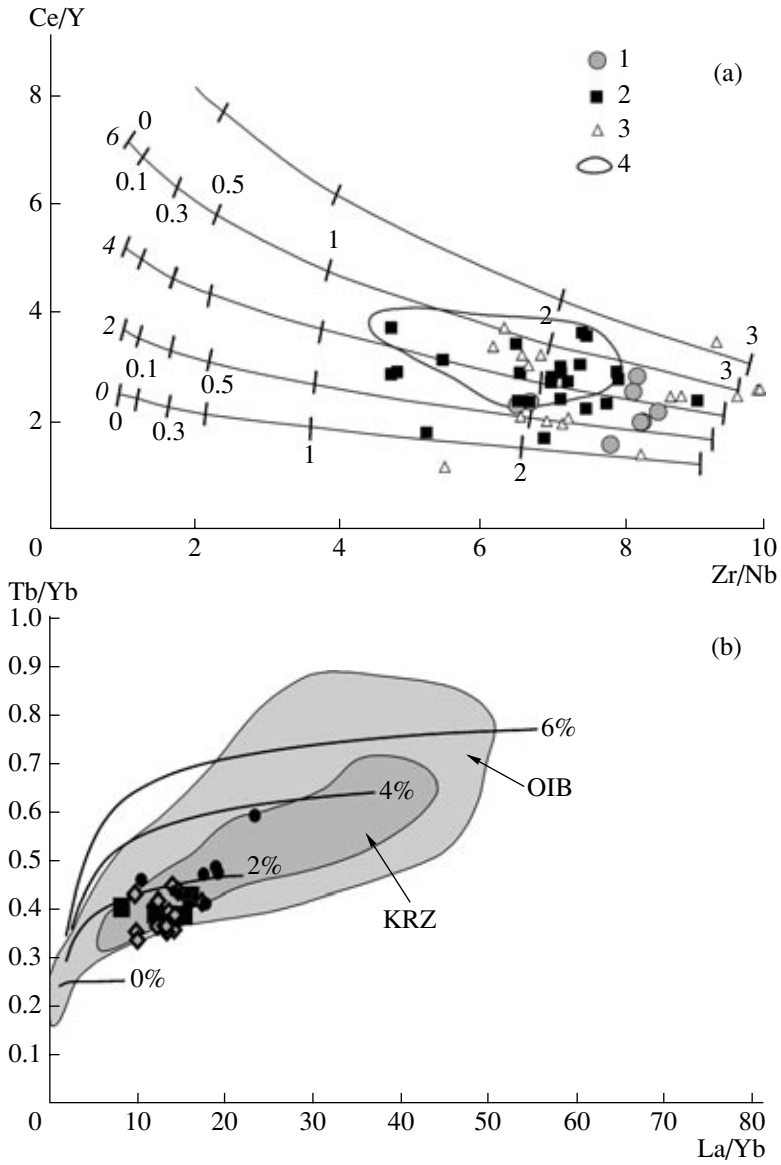

Fig. 9. Position of the basic rocks of the Vilyui rift in the diagrams Zr/Nb–Ce/Y and La/Yb–Tb/Yb, reflecting compositional variations of melts depending on the content of modal garnet and the degree of melting of the mantle source after (Rogers et al., 2000; Macdonald et al., 2001).

Solid lines correspond to melts derived from the mantle source with two times chondrite content of incompatible elements, numerals at the beginning of the lines show the garnet content. Numerals near transverse lines show the degree of melting, in percents.

(a) (1) moderate-Ti basic rocks, (2) high-Ti basic rocks, (3) basic rocks of the rift zones of the Altai–Sayan area after (Yarmolyuk and Kovalenko, 2003), (4) compositional field of alkali potassium basic rocks of post-kimberlite dikes.

(b) Symbols are as in Fig. 4. The gray field denotes the compositions of ocean island basalts (OIB) and basalts of the Kenyan rift zone (KRZ).

were produced at a higher degree of melting. It should be noted that post-kimberlite alkaline basalts, whose compositions are shifted toward higher garnet contents, were presumably formed at lower depth levels than the melts of the earlier stages. The same conclusion can be obtained using other criteria for estimating mantle melting conditions. In particular, the data points of the Vilyui rift cluster in the La/Yb–Th/Yb diagram (Fig. 9b) in the field of melts derived from garnet-bearing (~2%) mantle material. The post-kimebrlite basalts are distinguished from compositionally homogeneous rocks, and hence, the sources, are shifted toward mantle sources with higher contents of garnet. In Fig. 9, the rocks of the Vilyui rift plot in the compositional field of oceanic islands and Kenyan rift, typical occurrences of within-plate magmatism related to the activity of mantle hot spots.

Nature of magmatic sources. The compositional similarity between the magmatic rocks of the Vilyui rift

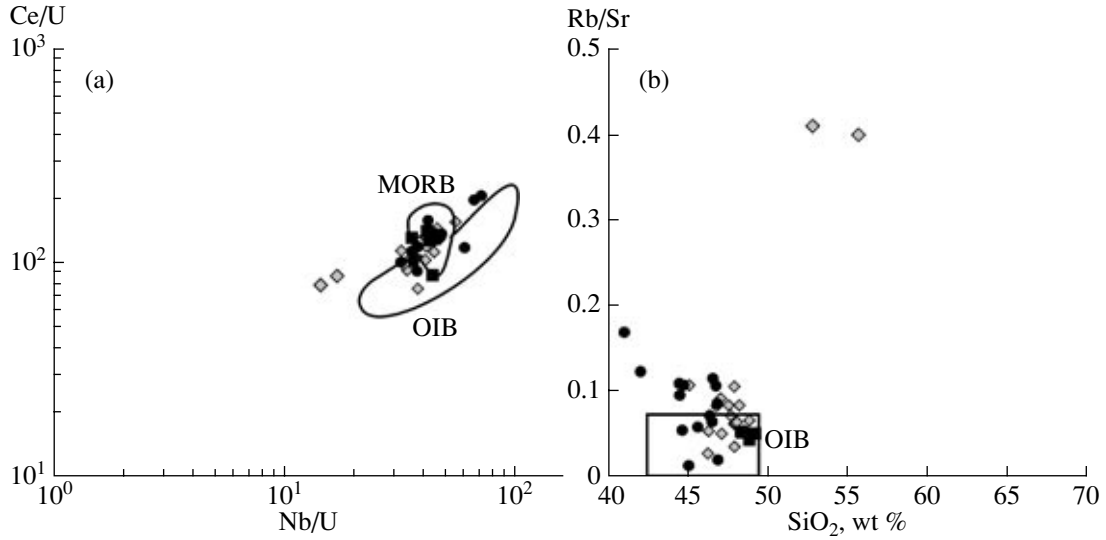

Fig. 10. Position of basic rocks in (a) Ce/U–Nb/U and (b) Rb/Sr–SiO_2 diagrams relative to the sources of MORB and OIBs. Symbols are as in Fig. 4.

and ocean island rocks is also seen in other indicator ratios of incompatible elements. In particular, the bulk of the basaltic rocks plot in Ce/U–Nb/U and Rb/Sr–SiO_2 diagrams in the OIB field (Figs. 10a, 10b). The Ce/U and Rb/Sr ratios are efficient tools for distinguishing between mantle and crustal sources (McDonough, 1999). The position of basalts in a Th/Ta–La/Yb diagram is shown in Fig. 11. The high Th/Ta ratios of mantle-derived rocks are typically considered to be related to the influence of crustal contamination or the participation of the recycled lithosphere in the mantle magma generation zones, whereas low Th/Ta and high La/Yb ratios are signatures of mantle sources in mid-ocean ridge and ocean island settings (Tomlinson and Condie, 2001). The basalts of the Vilyui rift plot within the OIB field, locating between a common component of mantle magmas of mid-ocean ridges and oceanic islands (FOZO) and enriched mantle sources (EMI, EMII, and HIMU). Based on the aforesaid indicator ratios, the magmatism of the Vilyui rift was classified with the OIB-type sources, whose appearance at the lithospheric base of the Siberian craton, as beneath oceanic islands, was related to plume activity.

In estimating the possible sources of the magmatic rocks of the Vilyui rift, special attention must be paid to their similarity with the rocks of the Middle Paleozoic rift zones of the Altai–Sayan system (Yarmolyuk et al., 2002). They are similar in petrochemical characteristics (high TiO_2 contents), the distribution of incompatible elements, and isotopic compositions (Figs. 7–9). In a Th/Ta–La/Yb diagram (Fig. 11), the basalts of the Altai–Sayan system, like the rocks of the Vilyui rift, fall in the OIB field, between FOZO and enriched mantle sources (EMI, EMII) (Tomlinson and Condie, 2001).

At the same time, these rocks are distinct from other within-plate rocks of different age within the Siberian platform and its nearby surrounding. Thus, we arrived at the conclusion that the basalts of the Vilyui and Altai–Sayan within-plate areas were derived from similar sources. Given that they were formed within compositionally and temporally heterogeneous continental crust, the contribution of continental lithosphere in the sources of these rocks was insignificant, with dominant role of mantle.

The composition of the upper regional mantle can be estimated on the basis of the composition of the magmatic rocks of ophiolite complexes in the Caledonian crust, which were derived by its melting and surround the Siberian platform practically on all sides. These rocks are MORB-type basalts with high ε_{Nd} (~+10) and low contents of trace elements (Yarmolyuk et al., 2002), indicating that the upper mantle could not be the source of the Middle Paleozoic basalts. The ophiolite complexes also contain OIB basalts, which have elevated TiO_2 contents and relatively low ε_{Nd} (~from +7 to +8). These basalts are interpreted as related to mantle plume activity (Kovalenko et al., 2005; Kovach et al., 2005) and, based on geochemical and isotope characteristics, are most similar to our rocks. Variations in composition, primarily, isotope composition, of the melting products of these plumes were presumably defined by the participation, along with PREMA, an additional phase, possibly, fluid, with an elevated $^{87}Sr/^{86}Sr$ ratio. To estimate the composition of this phase, we used data on the Altai–Sayan within-plate area, where magmatism occurred simultaneously with that in the Vilyui rift, and was characterized by a similar composition, suggesting their common source. In particular, isotope compositions of the rocks from both areas in the plot ε_{Sr}–ε_{Nd} show analogous relations. They plot above the mantle array, along upward concave mixing hyperboles, implying high and variable Sr/Nd

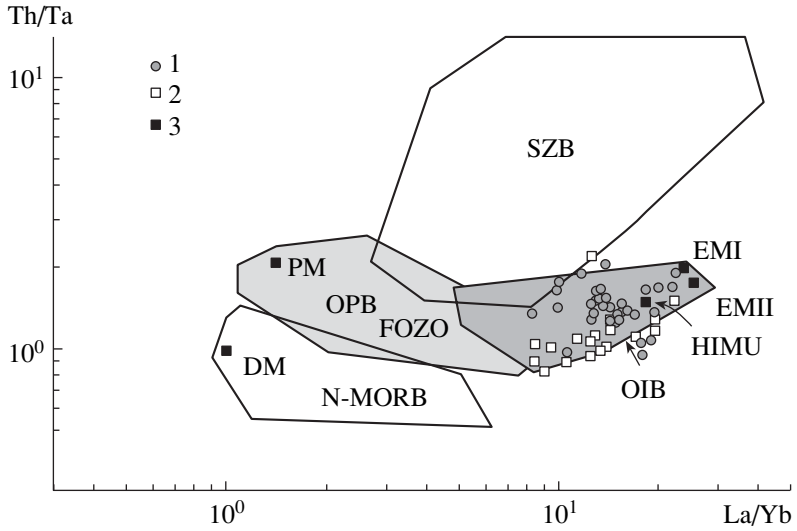

Fig. 11. Position of basic rocks of the Vilyui rift in the La/Yb–Th/Ta diagram (Tomlinson and Condie, 2001).
(1) Basic rocks of the Vilyui paleorift, (2) high-Ti riftogenic basic rocks of the Altai–Sayan area, (3) compositions of mantle sources. Fields of various types of basalts and some mantle sources: (OIB) ocean-island basalts, (OPB) oceanic plateau basalts, (N-MORB) mid-ocean ridge basalts, (SZB) subduction zone, (HIMU) source with high $^{238}U/^{204}Pb$ ratio, (EMI + EMII) the enriched mantle, (DM) depleted mantle, (PM) primitive mantle, (FOZO) the "focal zone" or the convergence zone of the isotope composition trends of the rocks of some ocean islands.

ratios in the source enriched in radiogenic Sr. This assumption is consistent with data on a positive correlation between the ε_{Sr} and Sr content, on the one hand, and between the ε_{Nd} and Nd content, on the other hand. In particular, as was mentioned above, the extremely high Sr isotope ratios (0.708–0.709), as well as high Ba and K contents, were found in the basalts with elevated Sr content (up to 3000 ppm) (Kiselev et al., 2002). These data indicate that one of the sources of the Devonian basalts, from which the rocks with high ε_{Nd} and negative ε_{Sr} values were derived, presumably corresponded to the moderately depleted PREMA mantle.

The second source (with high Sr isotope ratios) was characterized by elevated LILE contents and relatively low contents of other elements, including REE, which is typical of crustal sources, for example, those enriched in carbonate material. This suggests that the second source was related to the subducted lithosphere involved in recycling owing to plume activity. Based on experimental models of plume magma generation, up to 20% fragments of the subducted oceanic lithosphere must be contained in the plume head to explain the isotopic variations in OIB and large basaltic provinces, which could not be derived by the melting of homogeneous peridotite source (Takahashi et al., 1998).

Based on the aforesaid data, we propose the following model for the evolution of Middle Paleozoic magmatism and rifting in the eastern part of the Siberian platform (Kiselev et al., 2002; Kovalenko et al., 2005; Ernst and Buchan, 1997). In the Middle Paleozoic, the lithospheric plate of the platform and its folded framing were located above a hot mantle field, which fed at least two upper mantle plumes with compositionally similar products of magmatic activity. One of them was located at the base of eastern Siberia, while the other was beneath the southwestern margin of the platform (Fig. 12). The influence of both plumes on the lithosphere produced a triple junction rift system (Zonenshain et al., 1990; Kovalenko et al., 2005). This activity caused breakup along two branches of the rift system in the eastern part of the Siberian platform, while the third branch, directed inland, was preserved as the Vilyui rift. Decompressional melting presumably began when lithospheric ruptures reached the head of the mantle plume. The same ruptures further served as pathways for ascending basaltic magmas. To break the lithosphere, the plume must affect the lithosphere with a normal force equivalent to a 1–3 km rise of its base surface to initiate rifting (Arndt and Christensen, 1992). The rate of melting and the amount of melt generated by plume were determined by its excess temperature relative to the lithospheric mantle, as well as by the thickness and physical properties of the lithosphere. The large-scale Middle Paleozoic magmatic activity in the Siberian platform could be confined to the areas of ancient destruction, the Riphean aulacogens within the thinned and weakened lithosphere (Shpunt, 1987). The ascent of plume material beneath the thin lithosphere was accompanied by a high degree of partial melting and the formation of large volumes of basaltic melts. By contrast, the absence of decompression beneath the Archean terranes with a thick lithosphere caused the generation of lower degree melts. These conditions gave rise to melts corresponding to kimberlites and other alkali–ultramafic and alkali deep-seated rocks. The magmatic sequence established in the Vilyui–

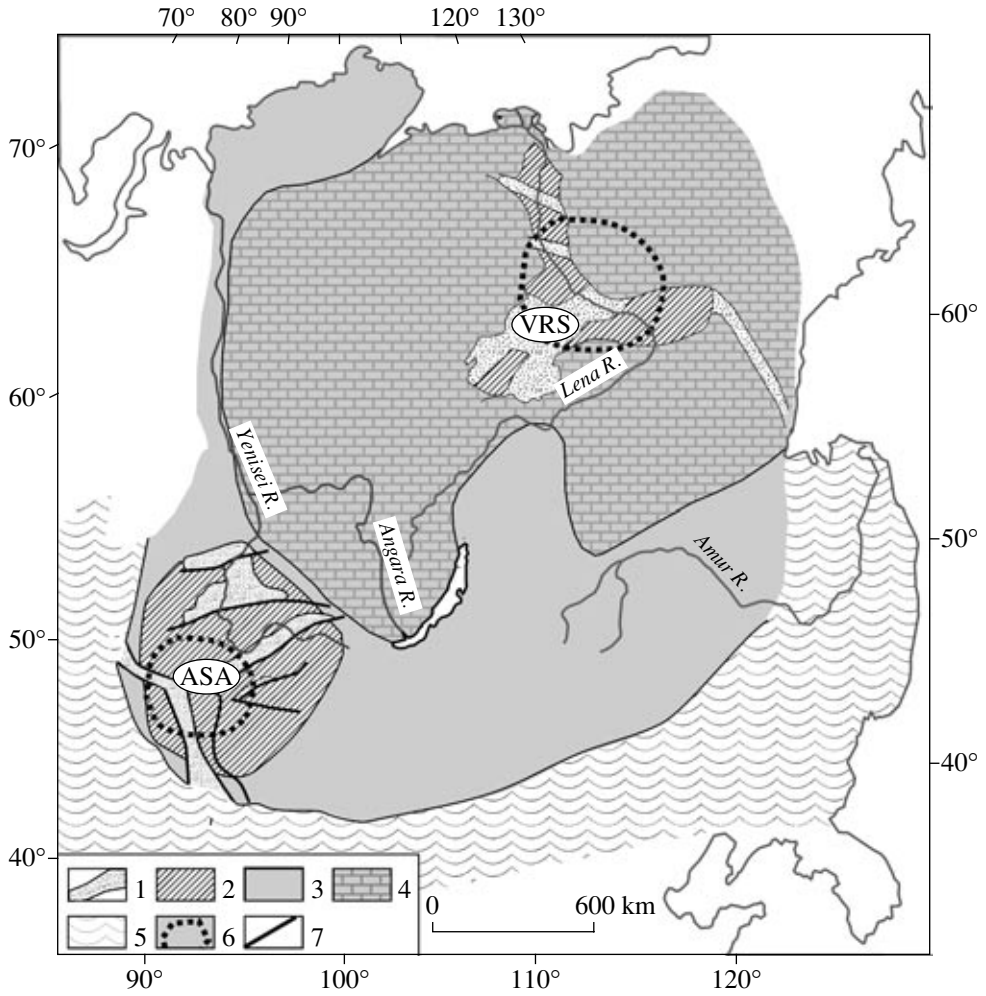

Fig. 12. Distribution of within-plate magmatism in the Middle Paleozoic Siberian paleocontinent.
(1) Volcanic depressions and grabens, (2) area of rises (shoulders of rift depressions and grabens), (3) territory of paleocontinent, (4) Siberian platform, (5) Paleo-Asian ocean, (6) projection of mantle plumes, (7) faults. (VRS) Vilyui rift system, (ASA) Altai–Sayan area.

Markha belt from large-scale basaltic eruptions spanning huge areas to limited kimberlite fields could be related to a decrease in the thermal activity of the plume with time and the deepening of the magma generation areas.

CONCLUSIONS

Middle Paleozoic magmatism in the eastern Siberian platform was related to riftogenic processes, which led to the formation of the Vilyui rift filled with sedimentary–volcanogenic sequences and the onset of extended basaltic dike belts on the rift shoulders. Two fields of diamondiferous kimberlites and basaltic dikes are located in the Vilyui–Markha belt, which surrounds the rift in the northwest. It was established that abundant subalkali basaltic magmatism predated the emplacement of kimberlite bodies, which occasionally (the Nyurba pipe) are cut by dikes of potassium alkaline basaltic rocks.

The petrography and geochemistry of the basaltic rocks testify that they could be derived by the fractionation of primary mantle melts during their ascent to the surface at insignificant crustal contamination. The melts were formed at fairly large depths, in the garnet stability field. The compositional differences between rocks formed in the rift depressions (moderate-Ti basalts) and in the cratonal framing of the rift (high-Ti basalts) were defined mainly by the degree of mantle melting. During the tectonic evolution of the Vilyui rift, the levels of mantle melting presumably deepened and the degree of melting decreased. As a result, the latest products became high in potassium, titanium, and incompatible elements.

The basalts of the Vilyui rift are compositionally similar to ocean island basalts and rocks of one of the most typical modern continental rifts, the Kenyan rift.

This similarity suggests their derivation from the same magmatic source, in particular, their relation to a mantle plume.

The geodynamic setting of Middle Paleozoic magmatism and rifting in the eastern part of the Siberian craton was controlled by plume–lithosphere interaction. The ascent of plume material to the base of the lithosphere, which was attenuated by Riphean destruction, was accompanied by decompressional melting and the formation of large volumes of exclusively basaltic melts. Plume ascent beneath the Archean terranes was limited by the thick lithosphere (up to 200 km and more), producing lower degree melts. This led to the formation of protokimberlite and other alkali ultramafic melts. The transitional zones between ancient stable blocks and Riphean aulacogens were characterized by the occurrence of both basaltic and kimberlite magmatism

ACKNOWLEDGMENTS

This study was supported by the Russian Foundation for Basic Research (project nos. 05-05-64043, 05-05-64000) and Program no. 10 of the Department of Earth Sciences, Russian Academy of Sciences "Central Asian Mobile Belt: Geodynamics and Stages of the Earth Crust Formation."

REFERENCES

1. A. M. Agashev, A. S. Fomin, T. Watanabe, and N. P. Pokhilenko, "Preliminary Age Determination of Recently Discovered Kimberlites of the Siberian Kimberlite Province, in *Proceedings of the 7th International Kimberlite Conference, Cape Town, South Africa, 1998* (Cape Town, 1998), pp. 9–10.
2. A. M. Agashev, N. P. Pokhilenko, A. V. Tolstov, et al., "New Age Data on Kimberlites from the Yakutian Diamondiferous Province," Dokl. Akad. Nauk **399**, 95–98 (2004) [Dokl. Earth Sci. **399**, 1142–1145 (2004)].
3. N. T. Arndt and U. Christensen, "The Role of Lithospheric Mantle in Continental Flood Volcanism: Thermal and Geochemical Constraints," J. Geophys. Res. **97** (B7), 10967–10981 (1992).
4. J. Blichert-Toft, C. E. Lesher, and M. T. Rosing, "Selectively Contaminated Magmas of the Tertiary East Greenland Macrodyke Complex," Contrib. Mineral. Petrol. **110** (1), 154–172 (1992).
5. R. E. Ernst and K. L. Buchan, "Giant Radiating Dyke Swarms: Their Use in Identifying Pre-Mesozoic Large Igneous Provinces and Mantle Plumes," in *Large Igneous Provinces: Continental, Oceanic and Planetary Volcanism*, Amer. Geophys. Union Geophys. Monogr. **100**, 297–333 (1997).
6. V. V. Gaiduk, *Middle Paleozoic Vilyui Rift System* (Yakutsk. Fil. Sib. Otd. Akad. Nauk SSSR, Yakutsk, 1988) [in Russian].
7. Sh. Gao, T.-Ch. Luo, B.-R. Zhano, et al., "Chemical Composition of the Continental Crust as Revealed by Studies in East China," Geochim. Cosmochim. Acta **62** (11), 1959–1975 (1998).
8. S. A. Gibbson, R. N. Thompson, A. P. Dickin, and O. H. Leonardos, "High-Ti and Low-Ti Mafic Potassic Magmas: Key to Plume Lithosphere Interactions and Continental Flood-Basalt Genesis," Earth Planet. Sci. Lett. **135** (3–4), 411–443 (1995).
9. C. J. Hawkesworth, N. W. Rogers, P. W. C. van Calsteren, and M. A. Menzies, "Mantle Enrichment Processes," Nature **311** (5984), 331–335 (1984).
10. C. J. Hawkesworth, P. C. Lightfoot, V. A. Fedorenko, et al., "Magma Differentiation and Mineralisation in Siberian Flood Basalts," Lithos **34** (1–3), 61–88 (1995).
11. A. D. Khar'kiv, N. N. Zinchuk, and V. M. Zuev, *History of Diamond* (Nedra, Moscow, 1997) [in Russian].
12. A. I. Kiselev, K. N. Egorov, R. A. Chernyshov, et al., "Occurrences of Fluid–Explosion Disintegration of the Basic Rocks in the Nakyn Kimberlite Field (Yakutian Diamondiferous Province)," Tikhookean. Geol. **23** (1), 97–104 (2004).
13. A. I. Kiselev, K. N. Egorov, and M. N. Maslovskaya, "Geodynamics of the Evolution of Kimberlite and Basic Magmatism in the Vilyui Rift Area," Otechestvennaya Geol., No. 4, 40–45 (2002).
14. V. P. Kovach, Ping Jian, V. V. Yarmolyuk, et al., "Magmatism and Geodynamics of Early Stages of the Paleoasian Ocean Formation: Geochronological and Geochemical Data on Ophiolites of the Bayan-Khongor Zone," Dokl. Akad. Nauk **404** (2), 229–234 (2005) [Dokl. Earth Sci. **404**, 1072–1077 (2005)].
15. V. I. Kovalenko, V. V. Yarmolyuk, O. Tomurtogoo, et al., "Geodynamics and Crust-Forming Processes in the Early Caledonides of the Bayanhongor Zone, Central Mongolia," Geotektonika, No. 4, 55–76 (2005) [Geotectonics **39**, 298–316 (2005)].
16. C. Y. Langmuir, "Geochemical Consequences of in Situ Crystallization," Nature **340** (6230), 199–205 (1989).
17. P. C. Lightfoot, C. J. Hawkesworth, J. Hergt, et al., "Remobilisation of the Continental Lithosphere by a Mantle Plume: Major-, Trace Element, and Sr-, Nd-, and Pb-Isotope Evidence from Picritic and Tholeiitic Lavas of the Noril'sk District, Siberian Trap, Russia," Contrib. Mineral. Petrol. **114** (2), 171–188 (1993).
18. R. Macdonald, N. W. Rogers, J. G. Fitton, et al., "Plume-Lithosphere Interactions in the Generation of the Basalts of the Kenya Rift, East Africa," J. Petrol. **42** (3), 877–900 (2001).
19. V. L. Masaitis, M. V. Mikhailov, and T. V. Selivanovskaya, *Volcanism and Tectonics of the Patom–Vilyui Aulacogen* (Nedra, Moscow, 1975) [in Russian].
20. M. S. Mashchak and M. V. Naumov, "Middle Paleozoic Basic Magmatism of the Nakyn Kimberlite Field and the Problem of Kimberlite Age," in *Efficiency of Prediction and Search of Diamond Deposits: Past, Present, and Future (Diamond—50)* (VSEGEI, St. Petersburg, 2004), pp. 224–226 [in Russian].
21. W. F. McDonough, "Constraints on the Composition of the Continental Lithospheric Mantle," Earth Planet. Sci. Lett. **101** (1), 1–18 (1990).
22. B. V. Oleinikov, *Geochemistry and Ore Genesis of the Platformal Basic Rocks* (Nauka, Novosibirsk, 1979) [in Russian].
23. J. A. Pearce, "The Role of Subcontinental Lithosphere in Magma Genesis at Destructive Plate Margins," in *Conti-*

nental Basalt and Mantle Xenolith, Ed. by C.J. Hawkesworth and H.J. Norry (Shiwa, Nantwich, 1983), pp. 230–249.

24. N. Rogers, R. Macdonald, J. G. Fitton, et al., "Two Mantle Plumes Beneath the East African Rift System: Sr, Nd and Pb Isotope Evidence from Kenya Rift Basalts," Earth Planet. Sci. Lett. **176**, 387–400 (2000).
25. R. L. Rudnick and D. M. Fountain, "Nature and Composition of the Continental Crust: A Lower Crust Perspective," Rev. Geophys. **33**, 267–309 (1995).
26. B. R. Shpunt, *Late Precambrian Rifting in the Siberian Platform* (Yakutsk. Fil. Sib. Otd. Akad. Nauk SSSR, Yakutsk, 1987) [in Russian].
27. S. S. Sun and W. F. McDonough, "Chemical and Isotopic Systematics of Ocean Basalts: Implications for Mantle Composition and Processes," in *Magmatism in the Ocean Basins*, Geol. Soc. Spec. Publ., No. 42, 313–345 (1989).
28. E. Takahashi, K. Nakajima, and T. L. Wright, "Origin of the Columbia River Basalts: Melting Model of a Heterogeneous Plume Head," Earth Planet. Sci. Lett. **162** (1), 63–80 (1998).
29. V. P. Tarabukin, A. N. Reimes, and I. V. Nefedova, "Estimation of the Erosion Level of Kimberlite in the Nakyn Field, Yakutia," Otechestvennaya Geol., No. 6, 84–87 (2003).
30. S. R. Taylor and S. M. McLennan, *The Continental Crust: Its Composition and Evolution* (Blackwell, Oxford, 1985; Mir, Moscow, 1988).
31. K. Y. Tomlinson and K. C. Condie, "Archean Mantle Plumes: Evidence from Greenstone Belt Geochemistry," in *Mantle Plumes: their Identification through Time*, Spec. Pap. **352**, 341–358 (2001).
32. M. D. Tomshin, A. I. Zaitsev, A. L. Zemnukhov, and A. G. Kopylova, "Character of the Emplacement of the Basic Rocks in the Nakyn Kimberlite Field, Yakutia," Otechestvennaya Geol., No. 4, 44–49 (2004).
33. M. D. Tomshin, A. S. Fomin, V. P. Kornilova, et al., "Characteristics of Magmatic Rocks in the Nakyn Kimberlite Field, Yakutian Province," Geol. Geofiz., No. 12, 1693–1703 (1998).
34. V. V. Yarmolyuk, V. I. Kovalenko, V. P. Kovach, et al., "Isotopic Composition, Sources of Crustal Magmatism, and Crustal Structure of Caledonides of the Ozernaya Zone, Central Asian Foldbelt," Dokl. Akad. Nauk **387**, 387–392 (2002) [Dokl. Earth Sci. **387**, 1043–1047 (2002)].
35. A. I. Zaitsev, V. P. Kornilova, A. S. Fomin, and M. D. Tomshin, "On the Age of Kimberlite Rocks of the Nakyn Field, Yakutia," in *Problems of Diamond Geology and Some Ways of their Solution* (Voronezh. Gos. Univ., Voronezh, 2001), pp. 47–54 [in Russian].
36. D. Z. Zhuravlev, I. V. Chernyshov, A. A. Agapova, and N. I. Serdyuk, "Precise Nd Isotope Analysis of Igneous Rocks," Izv. Akad. Nauk SSSR, Ser. Geol., No. 12, 23–40 (1983).
37. L. P. Zonenshain, M. I. Kuz'min, and L. M. Natapov, *Tectonics of Lithospheric Plates in the Territory of the USSR* (Nedra, Moscow, 1990) [in Russian].